

RESEARCH ARTICLE

DOI: 10.63221/eies.v1i01.73-92

Highlights:

- Distinct mineral compositions in both reservoirs affect porosity and weathering.
- Yan'an shows higher porosity but lower permeability due to weak pore connectivity.
- Weakly oil-wet Yan'an has rapid water cut rise, while water-wet Yanchang has a better flow.
- Differences in minerals and pore-throat structures impact reservoir quality.

Keywords:

Ordos Basin
Yan 10 and Chang3 reservoir
Reservoir characteristics
Main controlling factors
Zhenbei Oilfield

Correspondence to:

23221020234@stumail.xsyu.edu.cn.

Citation: Ma et al., 2025. Study on Reservoir Characteristic Differences between the Late Triassic Yanchang Formation and Early Jurassic Yan'an Formation in Ordos Basin: A Case Study from Zhenbei Oilfield in Southwestern Margin. Evidence in Earth Science, 1(01), 73-92.

Manuscript Timeline

Received	March 27, 2025
Revised	April 16, 2025
Accepted	April 22, 2025
Published	April 24, 2025

Academic Editor:

Haoyu Wang

Copyright:

Original content from this work may be used under the terms of the Creative Commons Attribution 4.0 licence. Any further distribution of this work must maintain attribution to the author(s) and the title of the work, journal citation and DOI.

Study on Reservoir Characteristic Differences between the Late Triassic Yanchang Formation and Early Jurassic Yan'an Formation in Ordos Basin: A Case Study from Zhenbei Oilfield in Southwestern Margin

Qi Ma^{1,2,3,*} and **Qiang Tong**⁴¹ School of Earth Sciences and Engineering, Xi'an Shiyou University, Xi'an, Shaanxi 710065, China² Shaanxi Key Laboratory of Petroleum Accumulation Geology, Xi'an Shiyou University³ No. 11 Oil Production Plant, Changqing Oilfield Company, Qingyang, Gansu 745000, China⁴ Research Institute of Petroleum Exploration and Development, PetroChina, Beijing 100083, China

Abstract As the Early Jurassic and Late Triassic reservoirs in the Ordos Basin enter stages of high water-cut and elevated recovery, it becomes essential to implement stratified development adjustments in mature oilfields. These adjustments should be guided by the principles of the "Anchor Project." The goal is to achieve an effective water shut-off control and optimize the injection-production process for commingled production. To improve reservoir differentiation and formulate sustainable production strategies efficiently, this study conducts a detailed comparative analysis of reservoir characteristics using the Yan 10 (Yan'an Formation) and Chang 3 (Yanchang Formation) reservoirs in Block M of the Zhenbei Oilfield along the southwestern margin of the basin. Through comprehensive core analysis and laboratory data, microscopic differences are revealed by integrating petrographic analysis, reservoir space, petrophysical properties, sensitivity, and waterflood seepage investigations. The findings demonstrate the following: Variations in interstitial material, with chlorite-dominated cements in Yan 10 and illite/kaolinite prevalent in Chang 3; Larger pore geometries and stronger microscopic heterogeneity in Yan 10, which results in higher porosity, while Chang 3 exhibits superior permeability; Wettability differences show that Yan 10 is weakly oil-wet, while Chang 3 is water-wet, with the latter displaying superior flow capacity and oil displacement efficiency, reflecting better pore-throat network connectivity. In conclusion, unlike the single pore-throat structure controlling the properties of Yan 10, the permeability of Chang 3 is more sensitive to pore-throat geometry and microscopic heterogeneity, while porosity is less affected. This research enhances theoretical comprehension for formulating strategies for reservoir-specific development modifications in mature oilfields.

1. Introduction

The Ordos Basin, a multi-cycle superimposed basin in central China, has long been a critical area for hydrocarbon exploration and development due to its extensive sedimentary sequences and substantial resource potential (He, 2022; Fu et al., 2013). Recent advancements in petroleum geology theories and technologies have markedly improved the comprehension of intricate reservoir systems, resulting in breakthroughs in confirmed reserves and production efficiency (Liu et al., 2023; Zou et al., 2024). However, as mature oilfields within the basin transition into high water-cut and high-recovery stages, optimizing reservoir management strategies has become imperative to sustain production and maximize remaining oil recovery.

The Zhenbei Oilfield, situated on the southwestern margin of the Ordos Basin, exemplifies these challenges. Since its development in 2016, Block M of this oilfield has faced increasing reservoir heterogeneity and waterflooding conflicts, particularly within the Early Jurassic Yan'an Formation (Yan 10 member) and Late Triassic Yanchang Formation (Chang 3 member) (Zhang et al., 2014; Zhang et al., 2019; Zhang et al., 2020). Both formations serve as major oil-producing layers, yet their distinct depositional histories and diagenetic evolution have resulted in contrasting reservoir characteristics. The Yan'an Formation, deposited in fluvial-lacustrine environments, overlies the Yanchang Formation, which is formed in braided river settings influenced by tectonic uplift and erosion (Zeng et al., 2015; Li et al., 2020).

Previous studies have extensively investigated sedimentary controls, sandbody configurations, and hydrocarbon enrichment mechanisms in these reservoirs (Zhang et al., 2019; Hui et al., 2018; Zhang et al., 2021). However, a systematic comparative analysis of their micro-scale reservoir properties—essential for guiding stratified development adjustments—remains necessary. Current challenges in Block M include rapid water-cut rise, uneven pressure distribution, and suboptimal injection-production efficiency, all of which underscore the need for reservoir-specific strategies. For instance, the Yan 10 reservoir exhibits higher porosity but lower permeability compared to the Chang 3 reservoir, suggesting divergent pore-throat connectivity and fluid mobility (Zhang et al., 2021; Zhao et al., 2021). Furthermore, differences in mineral composition, wettability, and sensitivity further complicate production optimization (Shi et al., 2018; Yang et al., 2015). Addressing these issues requires a holistic understanding of how depositional, diagenetic, and structural factors collectively govern reservoir quality.

Therefore, this study focuses on the Early Jurassic Yan 10 and Late Triassic Chang 3 reservoirs in Block M of the Zhenbei Oilfield. Based on core samples from appraisal wells, extensive experiments were conducted, including casting thin sections, scanning electron microscopy, core analysis for porosity and permeability, capillary pressure curve testing, sensitivity tests, wettability tests, relative permeability testing, and oil-water displacement tests. Using the targeted reservoir data from these experiments, subsequent research was carried out to analyze the reservoir characteristic differences and their causes. By conducting detailed comparisons of petrology, petrophysical properties, pore-throat structures, and seepage capacity, the study aims to clarify the developmental characteristic differences between these two adjacent reservoirs, which share similar reservoir types. The findings will provide a foundation for addressing production sustainability challenges and optimizing production enhancement measures in the oilfield.

Specifically, this study aims to address the following scientific issues: 1) Differentiation and genesis of various reservoir micro-characteristics between the Chang 3 oil member of the Yanchang formation and the Yan'an 10 oil member of the Yan'an formation in the Ordos basin; 2) Impact and genesis of mineral composition differences on the formation of reservoir space; 3) Impact of micro-pore-throat structures on petrophysical properties and analysis of factors contributing to pore-throat heterogeneity.

2. Regional Geological Overview

The Ordos Basin is a multi-cycle, superimposed basin (He, 2022) that has experienced prolonged tectonic evolution. Based on its current morphological characteristics, the basin can be divided into six primary structural units (Fu et al., 2013) (Figure 1-a). The basin's margins are characterized by extensive faulting and folding, while the interior Shaanbei Slope exhibits a relatively gentle gradient. Under long-term stable conditions, the basin displays a monoclinical structure that dips from southeast to northwest (Li et al., 2022). The Zhenbei Oilfield is situated on the southwestern margin of the Ordos Basin, positioned at the edge of the Yishan Slope tectonic belt. It spans the Tianhuan Depression and is geographically located in the Longdong region of Gansu Province.

The M area, situated in the central-eastern section of the oilfield, exhibited braided river deposits during the Yan 10 period and frontal deposits during the Chang 3 period, with sediment sources continually emanating from the northeast. A comprehensive analysis of core observations, well logs, sedimentary structures, and grain size data reveals that the Yan 10 Formation consists of braided channel, floodplain, and point bar microfacies, while the Chang 3 Formation is characterized by subaqueous distributary channels, interdistributary bays, subaqueous levees, and crevasse splays. Exploration and development practices, particularly since the beginning of large-scale production, have confirmed that the primary oil-producing layers in Block M of the Zhenbei Oilfield are the Yan 10 and Chang 3 reservoirs, both developed using waterflooding. The Yan 10 reservoir includes a total of 50 wells, consisting of 36 producers and 14 injectors, while the Chang 3 reservoir has 95 wells, with 70 producers and 25 injectors. Development efforts have primarily focused on the Chang 3 reservoir of the Yanchang Formation (Figure 1-b).

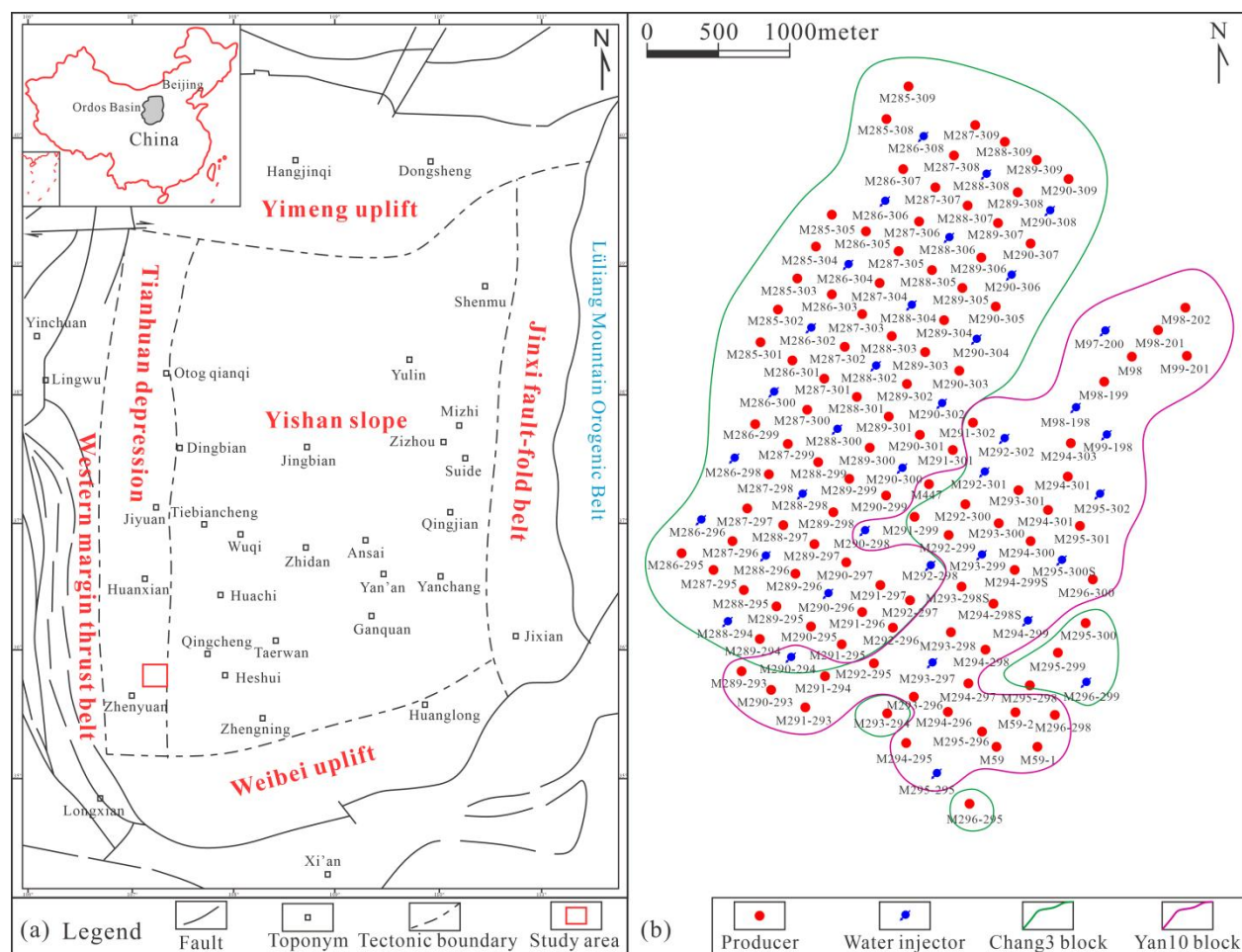


Fig. 1 a Structural division of the Ordos Basin and location of the study area; b Distribution of injectors and producers in the study area.

To date, the overall water cut of the reservoirs has approached 50%. The ongoing escalation in cumulative water injection correlates with a consistent rise in water cut, while the cumulative injection-production ratio is likewise progressively increasing. Furthermore, reservoir pressure remains excessively high, with localized high-pressure zones, leading to stress homogenization and a transition from unidirectional to multidirectional planar waterflooding, thereby intensifying waterflooding conflicts. In terms of productivity, the Chang 3 reservoir demonstrates higher per-well productivity than the Yan 10 reservoir, along with better waterflooding efficiency and actual recovery rates. Meanwhile, the comprehensive water cut and injection-production ratio of the Chang 3 reservoir are lower than those of the Yan 10 reservoir. According to reserve recalculations, the geological reserves of the Yan 10 reservoir are estimated at approximately 2.0286 million tons, while those of the Chang 3 reservoir are approximately 2.6234 million tons.

3. Materials and Methods

The experimental samples used in this study were sourced from core drilling data obtained from appraisal wells in the research area. All samples underwent standardized pretreatment: (1) cylindrical plugs (2.5 cm diameter × 5 cm length) were drilled perpendicular to the bedding planes; (2) residual hydrocarbons and salts were removed via Soxhlet extraction using toluene/methanol azeotrope (3:1 v/v) for 72 hours; (3) samples were oven-dried at 80 °C for 48 hours to reach a constant weight. The experimental results were provided by the Changqing Oilfield Branch, while the collection and organization of the sample data were carried out by the authors of this paper. The experiments conducted include thin section analysis, scanning electron microscopy, core analysis for porosity and permeability testing, mercury injection data analysis, sensitivity analysis, wettability analysis, relative permeability testing, and waterflooding oil recovery experiments. Details are as follows:

3.1. Thin Section Analysis

Petrographic characterization was carried out using a Leica DM4500P polarizing microscope. Cast thin sections (30 μm thickness) were prepared by vacuum-impregnating samples with blue epoxy resin (Araldite® CY 230) to highlight porosity. Grain size, sorting, mineral composition, and cement distribution were quantified using JMicroVision v1.3.4 software under 100–400× magnification, adhering to SY/T 5368-2016 (China Petroleum Industry Standard for Thin Section Analysis).

3.2. Scanning Electron Microscopy (SEM)

A FEI Quanta 650 FEG SEM equipped with an EDAX Octane Elite EDS detector was employed for observation. Samples were sputter-coated with 10 nm Au-Pd alloy to enhance conductivity. Imaging was conducted at 15 kV accelerating voltage, 10 mm working distance, and 5,000–20,000 × magnification. Secondary electron (SE) and backscattered electron (BSE) modes were used to characterize pore-throat morphology, clay mineral textures, and authigenic cements.

3.3. Porosity and Permeability Testing

Helium porosity (Φ) and gas permeability (K) were measured using a Coretest Systems AP-608 Automated Permeameter under 1.38 MPa confining pressure, following GB/T 29172-2012 (Chinese National Standard for Core Analysis). Each plug underwent three sequential measurements to ensure repeatability (error < ±2%).

3.4. High-Pressure Mercury Injection (HPMI)

Pore-throat size distribution was quantified using a Micromeritics AutoPore IV 9500 porosimeter. Samples were evacuated to 50 μmHg and mercury intrusion was performed up to 207 MPa, with Washburn equation parameters as: mercury surface tension 485 mN/m, contact angle 140°. Data interpretation followed SY/T 5346-2005 (Standard for Capillary Pressure Curve Analysis).

3.5. Sensitivity Analysis

Formation damage potential was evaluated via coreflooding experiments using a Hassler-type core holder (Temco X-1). Sensitivity tests followed the SY/T 5358-2010 protocols. Velocity sensitivity: Brine (10 g/L NaCl) injected at 0.1–3.0 mL/min, permeability damage ratio calculated; Water sensitivity: Permeability loss was measured after switching from synthetic formation water (TDS 35,000 ppm) to distilled water; Salt sensitivity: Salinity reduced stepwise from 35,000 ppm to 2,000 ppm, and permeability was monitored; Acid/alkali sensitivity: 15% HCl and 12% NaOH solutions were injected sequentially, and permeability was compared with the baseline.

3.6. Wettability Analysis

The Amott-Harvey wettability index (IW-O) was measured using a Coretest Systems SCAL-3 apparatus. Spontaneous imbibition of brine (0.5% NaNO₃) and crude oil (45°API) was monitored for 72 hours, followed by forced displacement at 0.5 mL/min. Index values were calculated according to the ASTM D1900-16.

3.7. Relative Permeability Testing

Steady-state oil-water relative permeability curves were generated using Coretest Systems UDS-300 rig. Experiments simulated reservoir conditions (45°C, 15 MPa), with synthetic brine (viscosity 0.45 cP) and degassed crude oil (viscosity 2.8 cP) injected at fractional flows from 0% to 100% water. Data normalization followed the Johnson-Bossler-Naumann (JBN) method.

3.8. Waterflooding Efficiency

Oil displacement efficiency was quantified via unsteady-state corefloods using a Temco FDS-350 system. Cores were saturated with crude oil, followed by brine injection at 1.0 mL/min until water cut reached 98%.

3.9 Pearson correlation analysis

A p-value less than 0.05 was used to conduct the Pearson correlation study in SPSS 27.0. The computed parameters of the Pearson correlation coefficient (r) from SPSS were transferred to GraphPad Prism 9.5 program to generate heat map diagrams. As shown in the heat map's legend, the value range encompasses two distinct ranges: red and blue, in which red represents a positive correlation and blue represents a negative correlation. A heat map that approaches red indicates a stronger positive correlation and a higher Pearson correlation coefficient. A heat map that trends towards blue indicates a stronger negative correlation, with the Pearson correlation coefficient approaching -1. When the correlation coefficient is 0 and the color is white, there is no significant correlation.

4. Results

4.1. Rock Types and Mineral Composition

In the study area, the Yan 10 reservoir is predominantly composed of lithic arkose, exhibiting relatively high compositional maturity. The grain size is primarily medium- to fine-grained sandstone, with localized occurrences of pebbly sandstone. The colors range from light gray to grayish-white (Figure 2). Sedimentary structures include massive bedding, parallel bedding, trough cross-bedding, and wedge-shaped cross-bedding. The interbedded mudstone is typically grayish-black or grayish-green in color.

In contrast, the Chang 3 reservoir, which was deposited during a lake contraction phase (Zhang et al., 2017), is mainly composed of feldspathic litharenite with lower compositional maturity. The sandstone grain size is similar to that of the Yan 10 reservoir, though it occasionally reaches medium-grained sandstone. Sedimentary structures are characterized by massive bedding, tabular cross-bedding, and horizontal bedding (Figure 2). The colors of the oil-bearing samples range

from grayish-white to brown. The interbedded mudstone is grayish-black and contains plant debris, suggesting a relatively humid and slightly oxidizing depositional environment.

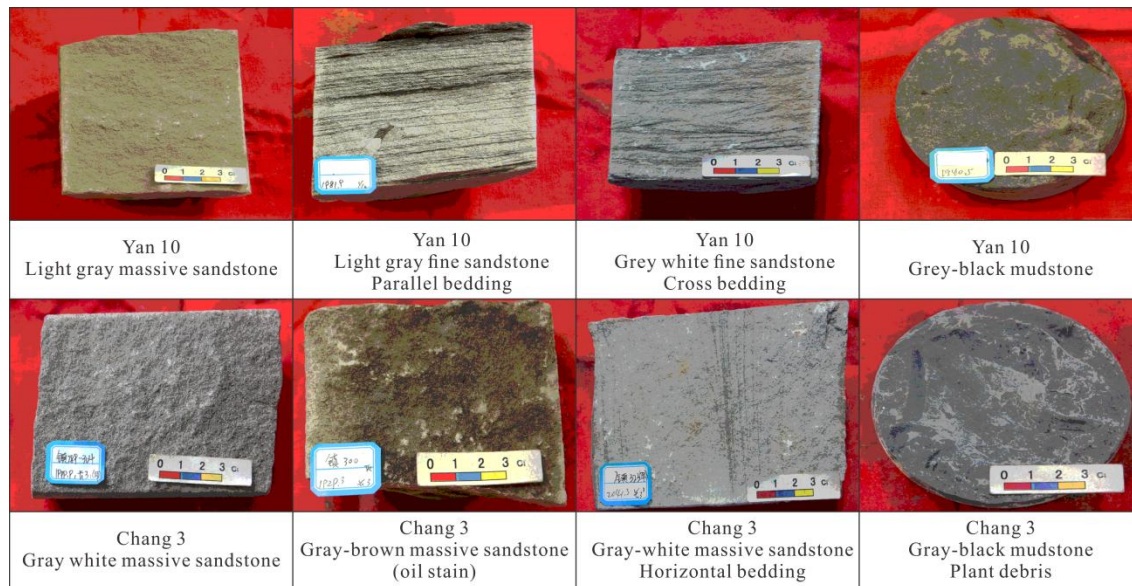


Fig. 2 Photographs of the Yan 10 oil-bearing of the Yan'an Formation and the Chang 3 oil-bearing of the Yanchang Formation in the study area.

A comparative analysis of the mineral composition reveals that the Yan 10 reservoir consists of 52.7% quartz, 18.8% feldspar, 14.6% rock fragments, and 13.9% interstitial material. In contrast, the Chang 3 reservoir contains 41.2% quartz (slightly lower than Yan 10), 13.4% feldspar, 33.4% rock fragments, and 12% interstitial material. This difference reflects the weaker hydrodynamic conditions during the deposition of subaqueous distributary channel sands in the Chang 3 period, compared to the braided channel sands of the Yan 10 period. The resulting conditions led to poorer sediment transport and lower compositional maturity (Figure 3-a).

The interstitial materials in the Yan 10 reservoir are primarily silica (4.3%) and kaolinite (4.0%), with smaller amounts of hydromica (2.0%) and ankerite (1.5%). In the Chang 3 reservoir, the interstitial materials are mainly hydromica (3.3%) and kaolinite (3.0%), followed by silica (2.8%) and ankerite (2.8%). As shown in Figure 3-b, while the types of interstitial materials are similar, their relative abundances differ significantly. Kaolinite, which predominantly fills intergranular pores, is more abundant in the Yan 10 reservoir, indicating higher pore-filling intensity. Additionally, hydromica, a product of the weathering and erosion of aluminum- and magnesium-rich rocks, reflects varying degrees of weathering and erosion in the two formations, which primarily affect the reservoir quality by damaging the pore spaces (Zhao et al., 2021).

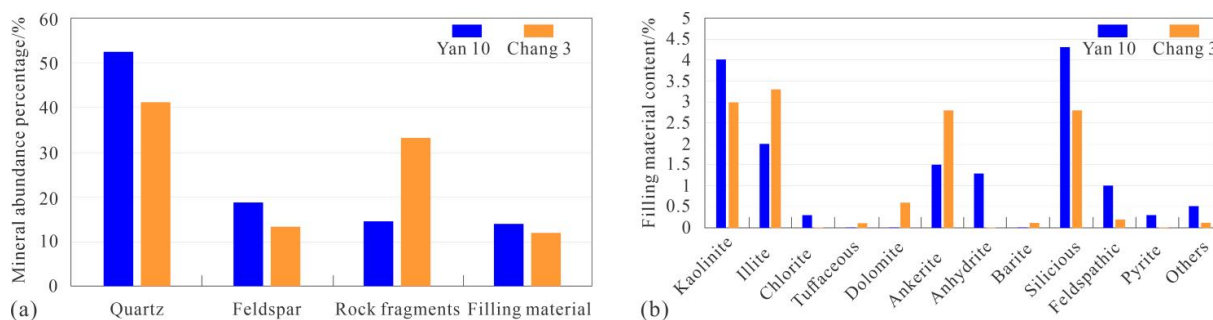


Fig. 3 a Comparison of Mineral Component Content; b Comparison of Interstitial Material Content.

4.2. Microscopic Rock Structure

Based on cast thin section and scanning electron microscopy (SEM) analyses, the microscopic rock structural characteristics of the Yan 10 and Chang 3 reservoirs in Block M were examined. The Yan 10 reservoir exhibits moderate to good sorting, subangular to subrounded grain shapes, and pore-filling cementation with overgrowths. In contrast, the Chang 3 reservoir demonstrates good sorting, predominantly subangular grain shapes, and similar pore-filling cementation with overgrowths (Figure 4).

Comparatively, the Chang 3 reservoir displays a higher level of structural maturity. The reservoir spaces are primarily characterized by secondary dissolution pores, although the influence of clay mineral filling (Yang et al., 2015) is evident, with intergranular spaces frequently filled by illite and kaolinite cement. Furthermore, clay mineral crystals attached to the grain surfaces alter pore throats and negatively impact fluid flow.

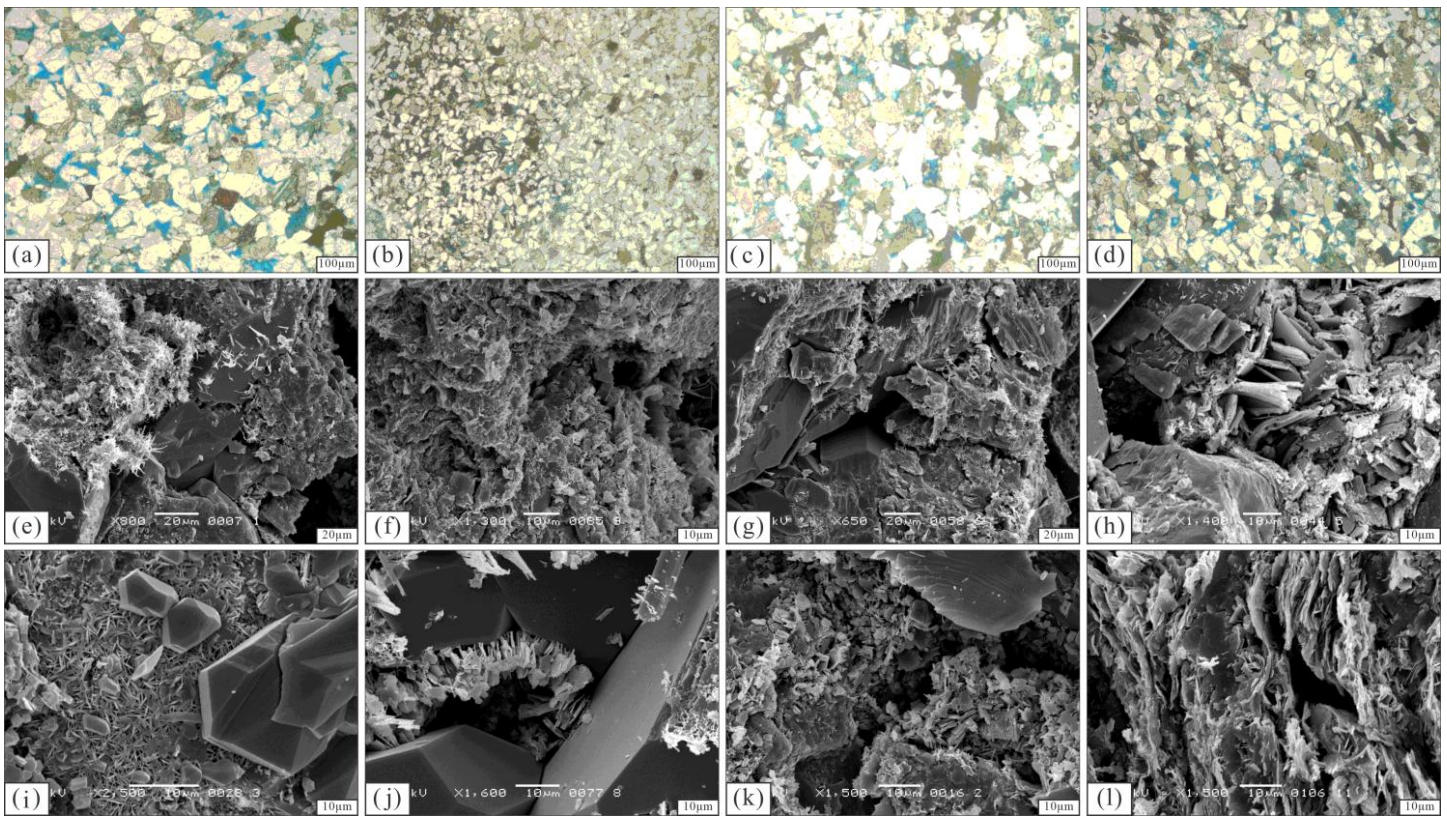


Fig. 4 Thin section and scanning electron microscopy analysis pictures of from Yan 10 and Chang 3 reservoirs in M area. (a: M447 Yan 10, 1978.2 m: Intergranular pores with chlorite rim cementation, subangular to subrounded structure; b: M323 Yan 10, 1897.14 m: Tightly packed quartz grains with localized intergranular dissolution pores, pore-blocking kaolinite cementation; c: M343 Chang 3, 2050.7 m: Dominant secondary dissolution pores with feldspar dissolution and quartz overgrowths, pore-blocking kaolinite and calcite cementation; d: M289-297 Chang 3, 1928.5 m: Well-sorted, subangular structure with dominant secondary dissolution pores, localized lithic fragments, and chlorite coatings; e: M447 Yan 10, 1978.2 m: Secondary quartz crystals and hair-like illite aggregates; f: M323 Yan 10, 1897.14 m: Localized intergranular dissolution pores with platy kaolinite crystals and filamentous/hair-like illite on grain surfaces; g: M294-288 Chang 3, 1994 m: Quartz overgrowths with localized hair-like illite on grain surfaces and intergranular pores; h: M286-296 Chang 3, 1873.5 m: Platy illite dissolution creating intergranular pores, chloritization forming leaf-like coatings on grain surfaces; i: M289-297 Chang 3, 1928.5 m: Leaf-like chlorite coatings and secondary quartz crystals; j: M300 Chang 3: Platy kaolinite filling secondary quartz intercrystalline pores; k: M59 Chang 3, 2057 m: Dissolution pores filled with platy kaolinite and localized hair-like illite; l: M343 Chang 3, 2050.7 m: Well-developed dissolution pores with platy illite lining detrital grains and chloritization forming leaf-like coatings.)

Based on cast thin section analysis and reservoir space data statistics, the Yan 10 reservoir is primarily characterized by dissolution pores and intergranular pores. In contrast, the Chang 3 reservoir displays a more diverse range of pore types, including dissolution pores, intergranular pores, and micropores, exhibiting a reduced overall pore area ratio (Figure 5).

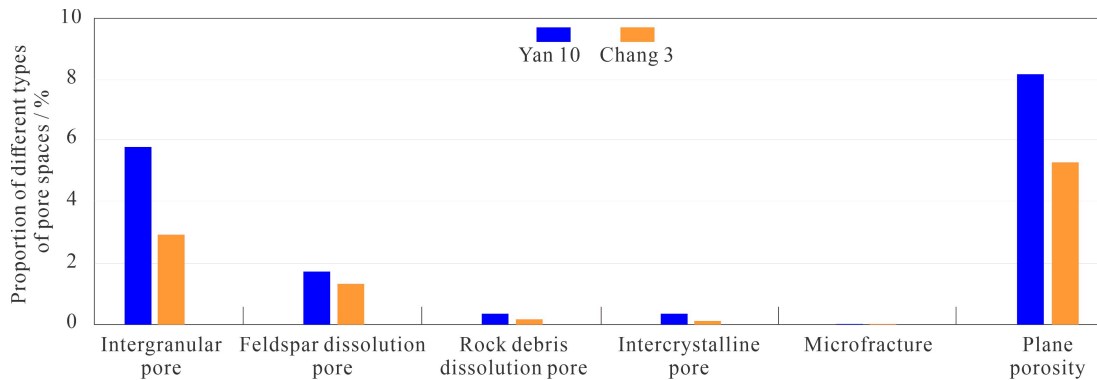


Fig. 5 Comparison of reservoir space types between the Yan 10 and Chang 3 reservoirs in the study area.

4.3. Pore-Throat Structure

Based on cast thin sections and image porosity analysis, the average pore diameter of the Yan 10 reservoir in Block M was measured 51.5 μm, with an average throat radius of 0.67 μm. In comparison, the Chang 3 reservoir has an average pore diameter of 57.7 μm and an average throat radius of 0.64 μm. Thus, the Chang 3 reservoir features relatively larger pores but smaller throats. According to the Ordos Basin throat classification standard, both reservoirs are categorized as medium-pore and fine-throat types.

High-pressure mercury injection (HPMI) data (Table 1) indicates that the Yan 10 reservoir has a lower average displacement pressure and median pressure than the Chang 3 reservoir, suggesting better development of larger pores and a relatively larger median radius. However, its average maximum mercury saturation is lower, implying poorer connectivity within the pore-throat network. The sorting coefficient, coefficient of variation, and skewness data further highlight stronger heterogeneity in the pore-throat structure of the Yan 10 reservoir. Among the sampled data, the Yan 10 reservoir shows slightly higher average porosity but lower average permeability compared to the Chang 3 reservoir.

Table 1. Comparison of high-pressure mercury injection parameters between Yan 10 and Chang 3 reservoirs in M area

Formation	Porosity (%)	Permeability (mD)	Displacement Pressure (MPa)	Median Pressure (MPa)	Median Radius (μm)	Maximum Mercury Saturation (%)	Withdrawal Efficiency (%)	Throat Sorting Coefficient	Variation Coefficient	Kurtosis	Skewness
Yan 10	13.2	3.025	0.2	1.62	0.47	92.95	41.05	2.09	0.22	3.38	1.39
Chang 3	11.67	3.2331	0.31	2.59	0.41	96.14	38.67	1.90	0.18	3.54	1.33

4.4. Petrophysical Properties

Based on core analysis results, both the Yan 10 and Chang 3 reservoirs are classified as low-porosity and ultra-low-permeability reservoirs. However, the Yan 10 reservoir demonstrates relatively higher porosity (Figure 6-a) but lower permeability (Figure 6-b), which is consistent with the previously observed differences in pore area ratio and throat radius. This indicates that the Yan 10 reservoir has larger pores but poorer pore-throat connectivity, resulting in enhanced storage capacity but weaker flow potential and lower fluid mobility.

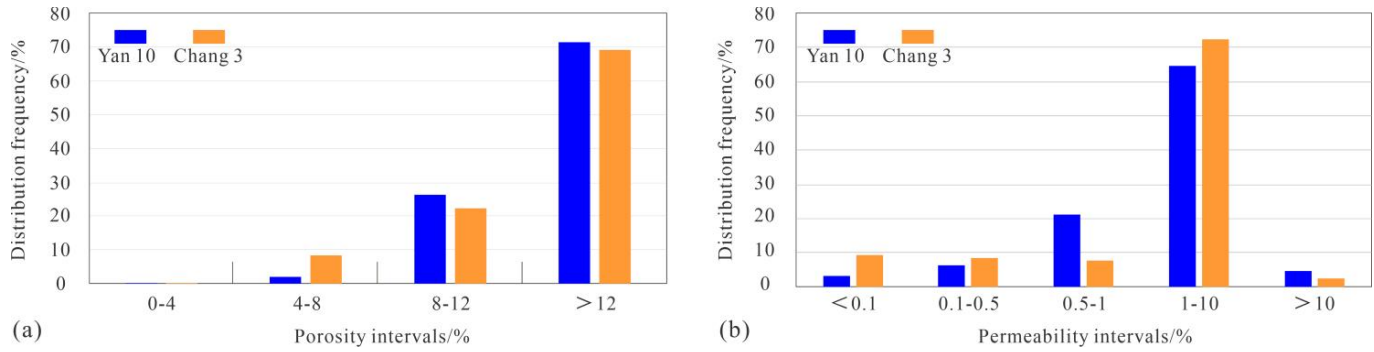


Fig. 6 a Porosity comparison of Yan 10 and Chang 3 reservoirs; b Permeability comparison of Yan 10 and Chang 3 reservoir.

4.5. Sensitivity Characteristics

The sensitivity analysis indicates that the Yan 10 and Chang 3 reservoirs in the research area demonstrate relatively negligible variations in alkalinity, acidity, and velocity sensitivity. However, there are significant differences in water and salt sensitivity (Table 2).

Table 2. Sensitivity difference analysis of Yan 10 and Chang 3 reservoirs in the study area

Sensitivity Type	Velocity Sensitivity	Alkali Sensitivity	Water Sensitivity	Acid Sensitivity	Salt Sensitivity
Yan 10	Moderately Strong	Weak	Moderately Strong	Moderately Strong	Moderate
Chang 3	Moderately Strong	Weak	Moderately Weak	Moderately Strong	Moderately Weak

The Yan 10 reservoir exhibits moderate water sensitivity, while the Chang 3 reservoir shows relatively weak water sensitivity. This suggests that the reservoir rocks in the Yan 10 reservoir absorb and retain water more rapidly, allowing for quicker water infiltration, which in turn affects the reservoir’s petrophysical properties and fluid characteristics. Additionally, the Yan 10 rocks have higher water conductivity, facilitating propagation and diffusion of water through the rock system (Shi et al., 2018).

In terms of salt sensitivity, the Chang 3 reservoir demonstrates relatively weak sensitivity, indicating greater stability during production and development. It shows stronger tolerance to saline water, with a lower likelihood of significant changes in reservoir properties or fluid dynamics due to saline water intrusion. Furthermore, the pore-throat structure of the Chang 3 reservoir is less susceptible to considerable alterations under varying saline water conditions (Zhang et al., 2023).

4.6. Wettability and Relative Permeability

Wettability measurements on representative samples show that the Yan 10 reservoir is predominantly weakly oil-wet, while the Chang 3 reservoir is neutral to weakly water-wet (Figure 7). The relative wettability index is -0.12 for the Yan 10 reservoir and 0.06 for the Chang 3 reservoir, indicating a notable difference in wettability between the two reservoirs.

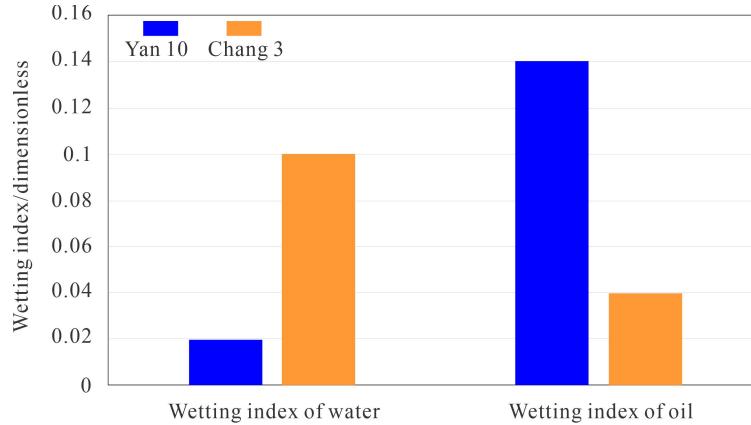


Fig. 7 Comparison of wettability between Yan 10 and Chang 3 reservoirs in the study area.

Relative permeability analysis of the Yan 10 and Chang 3 reservoirs reveals minor differences in irreducible water saturation, but the Chang 3 reservoir exhibits higher water saturation at residual oil (Figure 8).

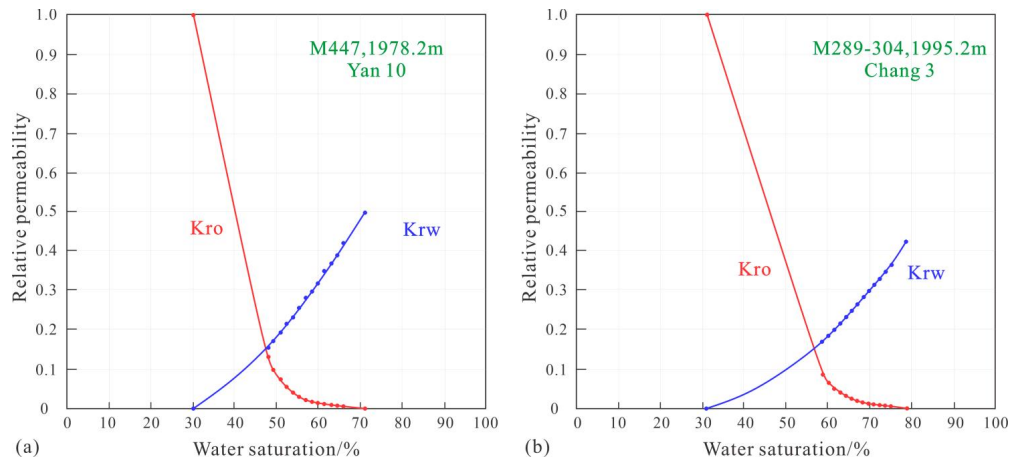


Fig. 8 Comparison of relative permeability curve characteristics of typical samples in the study area, a: sample from Yan 10 reservoir; b: sample from Chang 3 reservoir.

The findings indicate an expanded relative permeability zone and an increased co-permeability area for the Chang 3 reservoir, signifying enhanced oil-water relative flow capacity. The Yan 10 reservoir has elevated relative water permeability near the phase of residual oil, indicating a more rapid increase in water cut during the mid-to-late phases of waterflooding, necessitating meticulous management of water cut. Overall, the Chang 3 reservoir demonstrates a slower increase in water phase permeability and a slower decline in oil phase permeability, with the iso-permeability point shifting toward higher water saturation. These findings are consistent with the permeability comparison results, confirming the superior relative permeability characteristics of the Chang 3 reservoir.

4.7. Waterflooding Efficiency

Waterflooding experiments show that the oil displacement efficiency of both reservoirs increases significantly from the water-free stage to 95% water cut, 98% water cut, and ultimately to the final stage. However, the Yan 10 reservoir exhibits slightly lower displacement efficiency than the Chang 3 reservoir (Figure 9). For the selected samples, the Yan 10 reservoir has a slightly higher porosity (12.9%) compared to the Chang 3 reservoir (11.6%), while both reservoirs have similar permeability (3 mD). This suggests that, under comparable reservoir properties, particularly with identical

permeability, the Chang 3 reservoir demonstrates higher overall waterflooding efficiency, likely due to better connectivity in its pore-throat network.

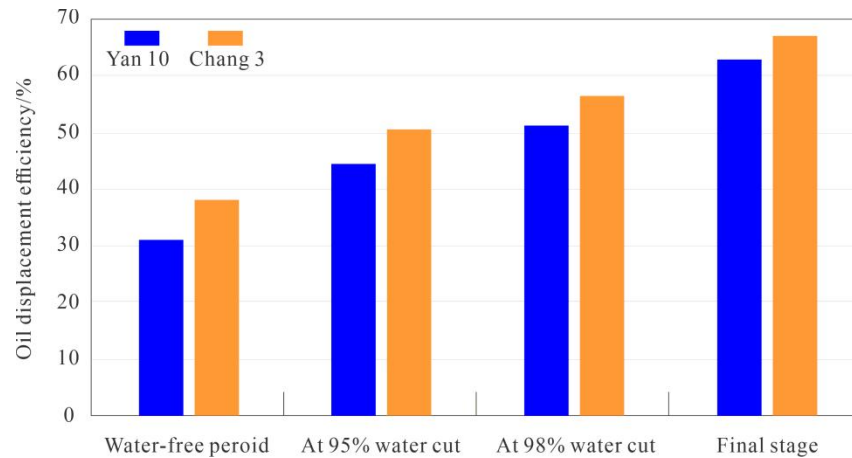


Fig. 9 Comparison of oil displacement efficiency of Yan 10 and Chang 3 reservoirs in the study area

The Results and Discussion section presents the findings of the study and interprets them in the context of existing literature and research questions. It should clearly highlight the main outcomes, explore their implications, and discuss any potential limitations or avenues for future research.

5. Discussion

5.1. Influence of Mineral Composition on Reservoir Space

Pearson correlation analysis was performed on the mineral composition and reservoir space types of the Yan 10 and Chang 3 reservoirs, producing correlation heatmaps where positive values indicate positive correlations and negative values indicate negative correlations. Correlations are considered significant when the Pearson correlation coefficient (r) is greater than 0.5 and the p -value is less than 0.05. The results reveal that in the Yan 10 reservoir, the parameter of plane porosity shows significant negative correlations with chlorite, ankerite, and other interstitial materials, indicating their detrimental effects on reservoir space (Figure 10-a).

The role of chlorite cements in pore-filling originates from the alteration of volcanic materials during the early diagenetic stage, which produces montmorillonite (Li et al., 2021). Volcanic and mica fragments undergo dissolution, releasing high concentrations of Mg^{2+} and Fe^{2+} , which leads to the precipitation of chlorite. Although chlorite significantly reduces the pore space in the reservoir, the chlorite content filling the pores in the Yan 10 reservoir is very low (Figure 3-b). Therefore, its destructive impact on reservoir properties is minimal.

Ankerite is a product of cementation, precipitating in pore spaces and filling primary intergranular pores or dissolution pores, which leads to a loss in pore connectivity. Although some ankerite forms minor authigenic micro-pores through replacement, its fibrous crystal morphology generally reduces the connectivity of intergranular pores (Yang et al., 2015), resulting in a primarily destructive effect on the pore space (Zeng et al., 2015). Other detrital material contents are also relatively low (Figure 3-b), making it difficult to significantly fill the pore space.

In contrast, the development of anhydrite in the Yan 10 reservoir has a constructive effect on pore connectivity, reflecting its anti-compaction properties. Additionally, the content of pyrite shows a positive correlation with pore connectivity, suggesting a relationship with sedimentary processes. Although the overall content of pyrite in the Yan 10 reservoir is extremely low, it indicates that the Yan 10 reservoir is developed in a fluvial-deltaic sedimentary environment, primarily controlled by river facies deposition. This suggests stronger hydrodynamic conditions and relatively coarse-

grained sedimentary deposits, which may lead to better-developed reservoir porosity, thereby creating a positive correlation with pore connectivity.

Furthermore, the relatively high content of silica also exhibits a certain positive correlation with pore connectivity. Quartz cementation typically occurs during the early diagenetic stages, and silica cement can enhance the intergranular support to a certain degree, thereby reducing the porosity loss caused by compaction during burial. This helps to preserve primary intergranular pores (He et al., 2021). Additionally, partial dissolution may occur when acidic diagenetic fluids pass through, forming secondary micropores (Zhang et al., 2017). However, locally, excessive cementation may block the pores (Yang et al., 2015), leading to an overall weak positive correlation.

In the Chang 3 reservoir, the pore area ratio exhibits the strongest negative correlation with dolomite, followed by hydromica and kaolinite (Figure 10-b). Despite the generally low dolomite content in the Chang 3 oil reservoir, its destructive effect on the pore space of the reservoir is relatively significant. Dolomitization typically occurs at various stages of diagenesis (Warren, 2000). Due to the influence of unconformities, it is speculated that besides the dolomitization during the middle to late diagenetic stages, there is also a dolomitization during the early diagenetic stage. Based on the results of correlation analysis, it is believed that dolomitization during the middle to late diagenetic stages plays the dominant role in the Chang 3 oil reservoir, leading primarily to the blockage of pore space.

There is also a weak negative correlation between kaolinite, illite, and the porosity of the Chang 3 reservoir. In terms of sedimentary origin, the Chang 3 oil reservoir was mainly formed during the Middle to Late Triassic period, characterized by significant changes in water depth and frequent hydrodynamic variations. As a result, the clay mineral content is relatively high, particularly illite, which is much more abundant than in the Yan 10 oil reservoir. This is related to the transformation from kaolinite. In terms of diagenetic evolution, the clay mineral cementation in the Chang 3 oil reservoir is relatively strong and has a more destructive effect on reservoir properties, being one of the major destructive diagenetic processes in the extended reservoir (Ma et al., 2015).

Furthermore, as shown in Figure 10b, the intergranular pores of kaolinite have a strong constructive effect on pore space. However, after being filled with fibrous illite, the connectivity of the intergranular pores decreases, which results in a destructive effect on the total porosity. On the other hand, the content of feldspar and other minerals shows a positive correlation with porosity. It is speculated that the constructive diagenetic effects related to feldspar dissolution have expanded the pore space through dissolution (Sun et al., 2022). However, considering the overall low content of these two mineral types, their effect on improving reservoir properties is not significant.

In both the Yan 10 formation and the Chang 3 formation, there is an overall similar correlation trend between the various types of reservoir space and mineral composition. Nonetheless, a comparison of the two reservoir zones reveals substantial disparities in the contributions of the dominant mineral types, which exhibit comparatively higher content percentages, to the different types of reservoir spaces.

Kaolinite, which tends to react easily with acidic solutions, is more likely to form and be preserved in relatively warm and humid environments. When the sedimentary environment is more acidic, the dissolution effect will lead to the dissolution of detrital particles and the development of pores. As a result, in the Yan 10 reservoir zone, which has undergone stronger dissolution, quartz and feldspar are more easily altered to kaolinite (Luo et al., 2021). This leads to a close relationship between kaolinite content and the development of dissolved detrital pores. In contrast, the Chang 3 reservoir zone in the Yanchang Formation, with its relatively neutral sedimentary environment, experiences weaker dissolution. Kaolinite is more likely to exist in crystalline form during sedimentation, when intergranular pores are better developed. Additionally, cementation is relatively stronger in this environment (Pang et al., 2021). The sedimentary environment of the Chang 3 reservoir zone is more alkaline, so under the influence of K^+ , kaolinite undergoes conversion to illite, which corresponds to the lake-delta sedimentary environment. Moreover, since the Chang 3 reservoir zone sediments were deposited earlier and have undergone stronger compaction, montmorillonite undergoes illitization as the

temperature increases (Tian et al., 2022), promoting the formation of illite. This is another factor contributing to the higher illite content in the Chang 3 reservoir zone.

Regarding ankerite, due to the good connectivity of the sand bodies in the Yan 10 reservoir zone and the relatively well-developed primary intergranular pores, a high-energy depositional environment can lead to poor sorting of detrital particles, which subsequently results in the filling of primary intergranular pores and dissolution pores by ankerite cement during later diagenesis (Pan et al., 2019). Ankerite also suppresses the dissolution during the middle to late diagenetic stage. In contrast, in the Chang 3 reservoir zone of the Yanchang Formation, the sand bodies are finer-grained, with relatively poor connectivity and fewer primary pores. However, the high organic matter content in this zone leads to the release of organic acids during hydrocarbon generation, which can promote dissolution, forming secondary pores. The formation of ankerite overlaps with the activity of organic acids, and under a locally weak alkaline environment, iron ions are more likely to precipitate as ankerite (Gao et al., 2019), forming a weak positive correlation.

Regarding siliceous clay, the relationship with reservoir space types shows minimal difference between the two reservoir zones. In the Chang 3 reservoir zone, a stronger negative correlation is observed between siliceous clay and intergranular pores, whereas in the Yan 10 reservoir zone, only a weak negative correlation exists. This is because the overall hydrodynamic conditions in the Chang 3 reservoir zone are relatively weak, and the clay content in the finer-grained sediments is relatively high. Moreover, under stronger compaction, the original pores are more easily filled by siliceous clay, which further restricts the development of secondary quartz enlargement and secondary intergranular pores (Zhou et al., 2017).

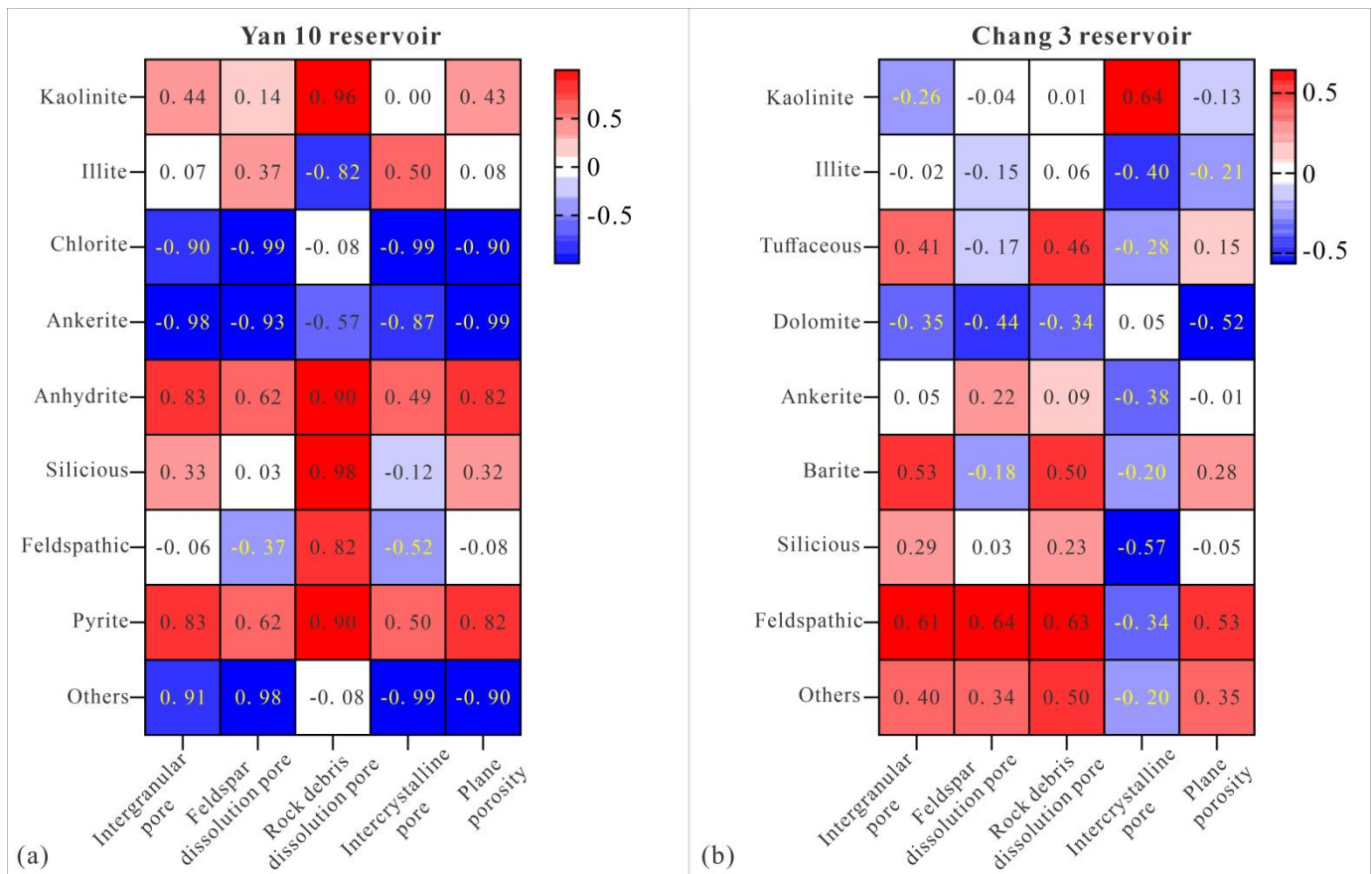


Fig. 10 a Heat map of the relationship between mineral composition and reservoir space in Yan 10; b Heat map of the relationship between Chang 3 mineral components content and reservoir space.

5.2. Influence of Pore-Throat Structure on Petrophysical Properties

The core analysis data and pore-throat structure parameters of the Yan 10 and Chang 3 samples were compiled, and correlation coefficient bar charts were created to compare pore-throat structure parameters with porosity and permeability. The analysis reveals that in the Yan 10 reservoir, parameters related to the displacement pressure, median pressure, and pore-throat radius have a relatively significant impact on the petrophysical properties (Figure 11-a). This is followed by parameters associated with heterogeneity, such as mercury withdrawal efficiency and the coefficient of variation (He et al., 2021). Specifically, pore-throat structure parameters in the Yan 10 reservoir exert a more significant influence on porosity, while their effect on permeability is comparatively weaker.

In the Yan 10 oil reservoir, the pore space of the rock is relatively large, as evidenced by the relatively low displacement pressure and median pressure. As a result, the pore-throat structure has a more significant impact on the reservoir properties. Additionally, due to the relatively good pore-throat connectivity, the Yan 10 oil reservoir exhibits a relatively high mercury injection efficiency (Table 1). Although the pore-throat structure has a slightly stronger control over porosity than permeability, the difference in correlation coefficients is not significant. Furthermore, the connectivity of the pore space is still somewhat hindered by clay minerals, such as kaolinite and chlorite (Zhao et al., 2021). This blockage, particularly when throat spaces are clogged with filling materials, is an important cause of the permeability decline (Sun et al., 2022). Therefore, overall, in the Yan 10 oil reservoir, the influence of the pore-throat structure on permeability is slightly lower than its influence on porosity.

Specifically, in the Yan 10 oil reservoir of the Yan'an Formation, parameters such as displacement pressure, median pressure, median radius, average throat radius, and average pore diameter are all strongly correlated with reservoir petrophysical properties. This reflects the relative advantages of the reservoir's storage space. However, it is also observed that the maximum mercury saturation is relatively poorly correlated with reservoir petrophysical properties. This is because the maximum mercury saturation parameter does not directly reflect the connectivity of the pores and the flow characteristics of the fluids within them. It is inferred that, to some extent, the complex effects of diagenesis on pore structure and permeability have resulted in larger disconnected pore regions in the reservoir's microstructure, which restrict fluid flow. Furthermore, the Yan 10 oil reservoir of the Yan'an Formation exhibits relatively good structural maturity and sorting (Meng et al., 2019), leading to smaller geometric size differences between large and small pores. As a result, parameters such as sorting coefficient show a weaker correlation with porosity and permeability.

In the Chang 3 oil layer of the Yanchang Formation, there are significant variations in the correlations between pore-throat structure parameters and both porosity and permeability. Specifically, the pore-throat structure parameters exhibit a weak influence on porosity, with correlation coefficients all being lower than 0.6. In contrast, the impact of these parameters on permeability is significantly stronger (Figure 11-b), which aligns with the general characteristics of the tight sandstone reservoirs in the Yanchang Formation of the Ordos Basin (Tong et al., 2022). This indicates that in such tight sandstone reservoirs, the influence of pore-throat structure on porosity is relatively weak, while its effect on permeability is more pronounced, especially in terms of the control exerted by pore-throat heterogeneity on permeability (Chang et al., 2025).

More specifically, among the parameters reflecting pore-throat size, parameters such as displacement pressure, average throat radius, median radius, and average pore diameter have a stronger control over reservoir permeability, but a weaker influence on porosity. This is because porosity is not the sole factor determining permeability, especially in tight sandstone reservoirs, where the connectivity between pores and throats and the heterogeneity of the pore-throat structure play a more significant role in controlling reservoir properties (Guo et al., 2024). As the pore structure becomes more heterogeneous, the connectivity between different types of pores decreases significantly, resulting in fluid being unable to flow through larger pore spaces, thereby enhancing the constraint on permeability. Therefore, for the Chang 3 oil layer with complex tortuosity, the coefficient of variation and pore-throat sorting coefficient also exert a strong control over permeability (Figure 11-b). Regarding the cementing material, the relatively high content of illite and siderite in the

Chang 3 oil layer can lead to a strong plugging effect on the throats (Zhong et al., 2021), further exacerbating the micro-heterogeneity between the pores and throats.

Comparatively, the control of pore-throat structure on reservoir petrophysical properties in the Yan 10 oil layer of the Yanchang Formation and the Chang 3 oil layer of the Yanchang Formation is generally similar. However, due to the differences in structural maturity, there are significant variations in skewness and tortuosity. Additionally, under the influence of differences in reservoir space (with Yan 10 having larger reservoir space and Chang 3 exhibiting stronger pore-throat heterogeneity), the Chang 3 oil layer is more strongly affected by these parameters. Mercury injection efficiency, as a representative parameter of pore-throat connectivity, also shows a weaker correlation with reservoir properties in the Chang 3 oil layer compared to the Yan 10 oil layer, likely due to the heterogeneity of the pore-throat structure. It is important to note that the two oil layers exhibit different correlation trends when it comes to maximum mercury saturation. This discrepancy is likely due to organic acid dissolution of feldspar and carbonate rock in the Chang 3 oil layer, forming honeycomb-like pores. However, uneven dissolution leads to poor pore connectivity, resulting in a higher proportion of isolated pores. As a result, mercury injection is less likely to achieve full saturation. Additionally, dissolution is accompanied by the transformation of clay minerals, particularly illitization, which forms a large number of nanopores, making it difficult for mercury to penetrate (Tian et al., 2022). This phenomenon is also related to the relatively lower energy of the lacustrine-deltaic depositional environment compared to fluvial facies.

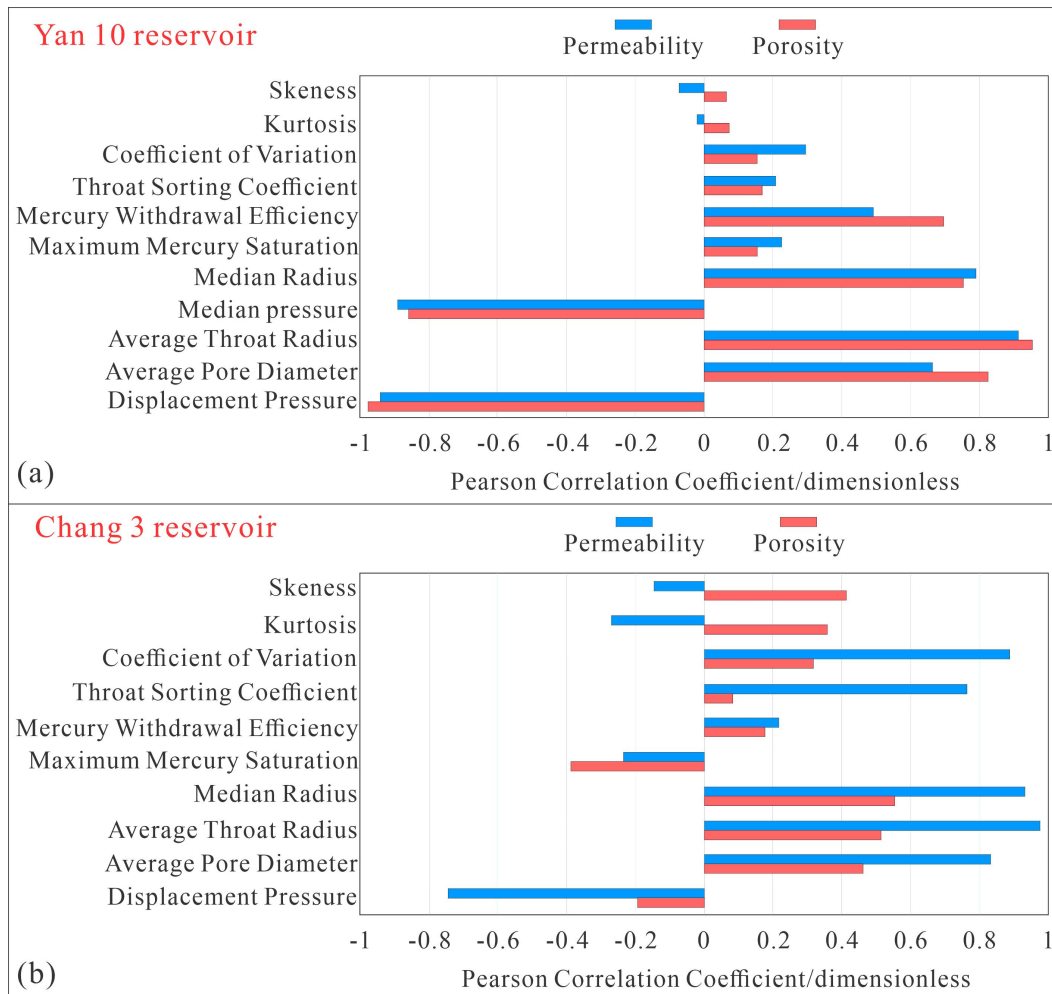


Fig. 11 a Influence of pore-throat structure parameters on petrophysical properties in the Yan 10 reservoir; b Influence of pore-throat structure parameters on petrophysical properties in the Chang 3 reservoir.

Pearson correlation coefficients were also applied to generate heatmaps that illustrate the relationships between pore-throat heterogeneity parameters in the Yan 10 and Chang 3 reservoirs (Figure 12a and 12b). In the Yan 10 reservoir, mercury withdrawal efficiency is most strongly influenced by the average throat radius and displacement pressure, with larger throat radii and lower displacement pressures leading to higher withdrawal efficiency. This is because the displacement pressure is primarily determined by the maximum connected throat radius. In the Yan 10 reservoir, the throats are predominantly sheet-like and bent-sheet-like in shape, with generally smaller throat radii. This is the main reason for the high displacement pressure. Additionally, small throats experience increases capillary resistance during mercury injection, which exacerbates the difficulty of mercury expulsion, significantly reducing the mercury withdrawal efficiency. Furthermore, the mercury expulsion efficiency is also controlled by the tortuosity of the throats.

Although the Yan 10 oil layer has a relatively larger pore volume compared to the Chang 3 oil layer, the throats in the Yan 10 oil layer are relatively narrower due to early carbonate and silicate cementation (Xiao et al., 2024). This is also the reason why the average porosity of the Yan 10 oil layer is higher than that of the Chang 3 oil layer, while its average permeability is slightly lower. Furthermore, a notable distinction between the Yan 10 and Chang 3 oil layers is that the reservoir in Yan 10 demonstrates pronounced water sensitivity (Table 2), whereas the wettability suggests that the reservoir predominantly displays an oil-wet feature (Figure 8a). Therefore, the displacement pressure of the non-wetting phase is bound to be higher. Similarly, parameters reflecting the geometric scale of pore-throats, such as average pore diameter, average throat radius, and median pressure, are closely related to mercury withdrawal efficiency.

The throat sorting coefficient and variation coefficient exhibit weaker relationships with pore-throat structure parameters; however, they still indicate a tendency of decreasing pore and throat radii with increasing heterogeneity (Figure 12a). The maximum mercury injection saturation parameter shows a high correlation with the heterogeneity parameters representing pore-throat structure. It is significantly correlated with throat sorting coefficient, variance coefficient, skewness, and kurtosis, with correlation coefficients ($|r|$) around 0.5. This is because the maximum mercury injection saturation is primarily constrained by the proportion of fine throats, rather than the total pore volume. Therefore, the complexity of the throats directly determines the efficiency of mercury injection, especially in low-permeability reservoirs. The sorting and distribution patterns of the throats determine the range of capillary pressure thresholds, which further restrict the fluid flow within the reservoir (Li et al., 2022). As a result, the heterogeneity parameters of the throats exhibit a significantly stronger correlation with mercury injection saturation than parameters reflecting pore scale.

In the Chang 3 reservoir, parameters related to pore-throat radius, such as median radius, average pore diameter, and average throat radius, exhibit significant positive correlations with both the throat sorting coefficient and variation coefficient. This suggests that greater pore-throat heterogeneity is associated with larger pore-throat geometric dimensions and lower displacement pressure (Figure 12b).

For tight sandstone reservoirs, the difference in the proportion of large, medium, and small pore throats is of great significance in characterizing the sorting characteristics of the reservoir, especially the contribution of large pore throats, which make up a very small percentage of the total. These large pore throats contribute significantly to the reservoir porosity (Tong et al., 2022), and thus lead to an increase in the sorting and variation coefficients between large and small pore throats. The parameters reflecting the pore size distribution, however, have a relatively weak influence on skewness and tortuosity. This is primarily because these parameters are mainly controlled by throat size, not pore size. This behavior resembles that of the Yan 10 oil-bearing component, rendering further explanation superfluous.

As for the maximum mercury injection saturation parameter, it is observed that, unlike the Yan 10 oil-bearing member, this parameter has a significant negative correlation with skewness and tortuosity. This is due to the fact that the Chang 3 reservoir has undergone strong mechanical compaction and carbonate cementation, which has compressed the original intergranular pores. The average pore size difference is smaller, the throats are generally flattened and their sizes tend to converge, and the skewness of the throat morphology is largely controlled by the distribution of the primary cements. As a result, the sorting coefficient variation is relatively small. This also explains why the average porosity of the Chang 3 reservoir is relatively low, but its average permeability is still higher than that of the Yan 10 reservoir. Additionally, the

reduced effective flow pathways, influenced by the higher tortuosity, lead to a decrease in the maximum mercury injection saturation (Liu et al., 2022).

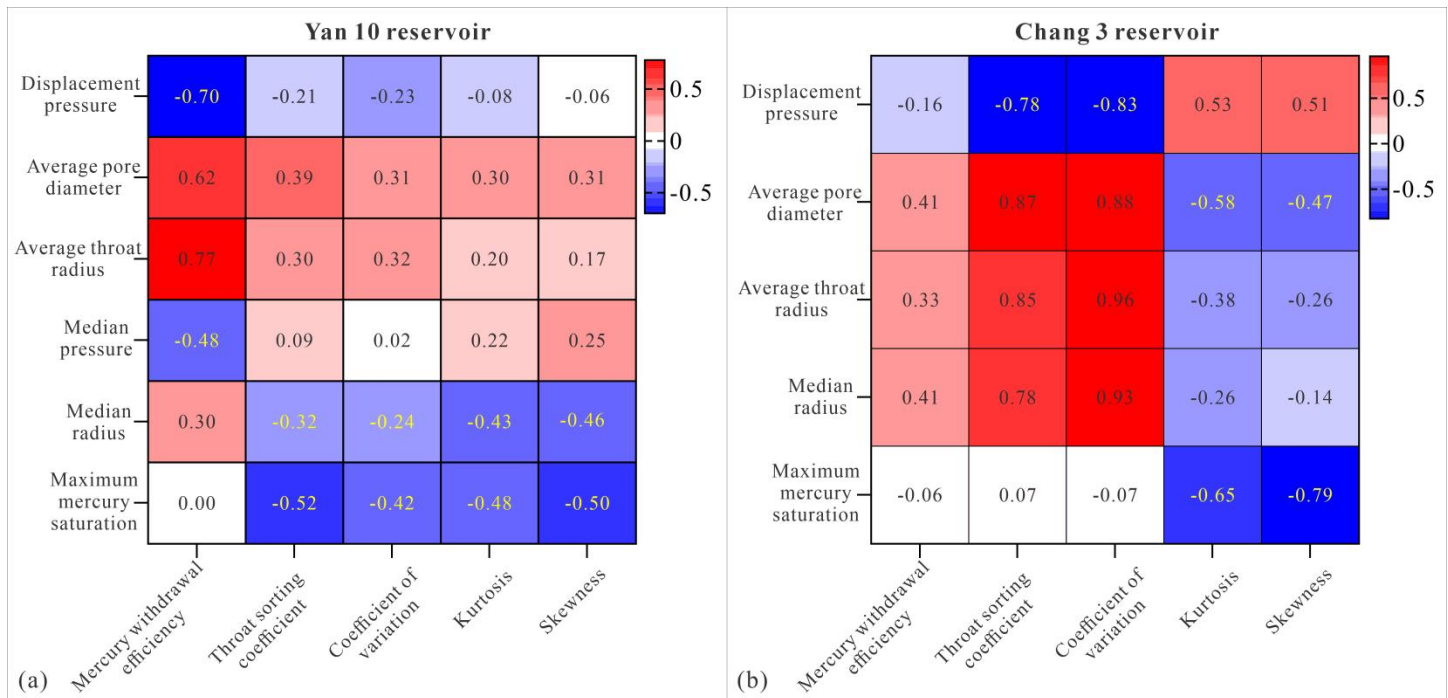


Fig. 12 a Heatmap of pore-throat heterogeneity parameter relationships in the Yan 10 reservoir; b Heatmap of pore-throat heterogeneity parameter relationships in the Chang 3 reservoir.

6. Conclusion

The main findings of this research are as follows;

1. The Yan 10 reservoir (lithic arkose, high compositional maturity) and Chang 3 reservoir (feldspathic litharenite) exhibit contrasting mineral composition—silica and kaolinite dominate Yan 10, while illite and kaolinite prevail in Chang 3. Microscopically, chlorite distribution diverges: pore-filling in Yan 10 versus surface-coating in Chang 3, with reduced kaolinite cementation in the latter intensifying pore-throat heterogeneity.

2. In terms of pore-throat structure, the Yan 10 reservoir has slightly larger pore-throat dimensions and better-developed macropores, though with poorer connectivity. The sorting and variation coefficients, which reflect differences in pore-throat scales, are higher in the Yan 10 reservoir. This leads to higher average porosity but lower permeability compared to the Chang 3 reservoir.

3. Wettability analysis indicates that the Yan 10 reservoir is weakly oil-wet, while the Chang 3 reservoir is neutral to weakly water-wet. Relative permeability measurements suggest that the Chang 3 reservoir exhibits stronger flow capacity, a slower rise in water cut, and higher ultimate displacement efficiency, which reflects the enhanced connectivity of its superior pore-throat network.

4. The controlling factors of reservoir properties differ significantly between the two reservoirs. The storage capacity of the Yan 10 reservoir is influenced by chlorite filling, while the Chang 3 reservoir is largely unaffected by this factor and is instead controlled by dolomite, illite, and kaolinite cementation. Consequently, the size of the reservoir space is influenced by different rock mineral compositions. Regarding the impact of pore-throat structure on petrophysical properties, the Yan 10 reservoir demonstrates simpler relationships, whereas the Chang 3 reservoir exhibits a stronger correlation between pore-throat geometric dimensions and permeability than with porosity. Furthermore, pore-throat

heterogeneity parameters have a significant influence on the permeability of the Chang 3 reservoir, unlike in the Yan 10 reservoir. A comparative analysis of pore-throat structural differences reveals opposing trends in how geometric dimensions influence the intensity of microscopic heterogeneity in each reservoir

Author Contribution

Qi Ma: Conceptualization, Data curation, Formal analysis, Funding acquisition, Investigation, Methodology, Project administration, Resources, Software, Supervision, Validation, Writing-original draft; Qiang Tong: Visualization, Writing-review& editing.

Acknowledgements

The author gratefully acknowledges the funding and assistance from proof-readers and editors. And the author would like to acknowledge the support of the Shaanxi Provincial Natural Science Foundation Project "Quantitative Characterization of Micro-Nano Pore-Throat Systems in Shale Oil Reservoirs and Their Control Mechanisms on Movable Fluid Occurrence States" (Grant No. 2022JQ-290).

Conflict of Interests

The authors declare no conflicts of interest.

Data Availability

The data supporting the findings of this study are available upon request from the corresponding author.

References

- Chang, B., Tong, Q., Cao, C., et al. (2025). Effect of pore-throat structure on movable fluid and gas–water seepage in tight sandstone from the southeastern Ordos Basin, China. *Scientific Reports*, 15: 7714. DOI: 10.1038/s41598-025-92584-7.
- Fu, J.H., Li, S.X., Liu, X.Y. (2013). Geological theory and practice of petroleum exploration in the Ordos Basin. *Natural Gas Geoscience*, 24(06), 1091-1101.
- Gao, Y., Liu, C., Bai, X.J., et al. (2019). Cement characteristics of overgrown authigenic ferron dolomite and its impact on tight sandstone reservoirs qualities: Case study of the Chang 4 & 5 members of Triassic Yanchang Formation in Longdong area, Ordos Basin. *Oil and Gas Geology*, 40(05), 1065-1073. DOI: 10.11743/ogg20190512.
- Guo, C.F., Li, A.R., Fan, W.H., et al. (2024). Micro-pore structure of tight sandstone reservoir and influence on reservoir petrophysical properties: Chang 6 Member of Huangling Area, Ordos Basin as an example. *Science Technology and Engineering*, 24(34), 14623-14631.
- He, D.F. (2022). Multi-cycle superimposed sedimentary basins in China: Formation, evolution, geologic framework and hydrocarbon occurrence. *Earth Science Frontiers*, 29(6): 24-59. DOI: 10.13745/j.esf.sf.2022.8.1.
- He, H., Zhou, Y.Q., Long, W.J., et al. (2021). Pore throat microstructures of low-ultra-low permeability reservoirs and their influence on water displacement characteristics: Taking the Chang 3 reservoir of Weibei Oilfield in Ordos Basin as an example. *Petroleum Geology and Recovery Efficiency*, 28(04), 23-34. DOI: 10.13673/j.cnki.cn37-1359/te.2021.04.003. DOI: 10.13673/j.cnki.cn37-1359/te.2021.04.003.
- Hui, W., Liu, Y.C., Wang, L.G., et al. (2018). Factors affecting the petrophysical property of Chang 3 reservoir in Yanwu oilfield of Ordos Basin. *J MINERAL PETROL*, 38(03), 113-120. DOI: 10.19719/j.cnki.1001-6872.2018.03.14.
- Li, K., Xi, K.L., Cao, Y.C., et al. (2021). Chlorite authigenesis and its impact on reservoir quality in tight sandstone reservoirs of the Triassic Yanchang formation, southwestern Ordos basin, China. *Journal of Petroleum Science and Engineering*, 205:108843-108843. DOI: 10.1016/j.petrol.2021.108843.

- Li, M., Liao, J., Wang, S., et al. (2022). Imbibition characteristics and influencing factors of reservoirs with ultra-low permeability Ordos Basin: A case study of the third member of Triassic Yanchang Formation in Weibei Oilfield. *Petroleum Geology & Experiment*, 44(06), 971-980. DOI: 10.11781/sydz202206971.
- Li, Y.H., Yang, G.R., Peng, J., et al. (2020). Formation and evolution of pre-Jurassic paleogeomorphology and characteristics of sedimentary filling in Ordos Basin. *Global Geology*, 39(01), 56-71. DOI:10.3969/j.issn.1004-5589.2020.01.005.
- Liu, C., Chen, G.H., Lu, Y.Y., et al. (2022). Micro pore throat structural characterization of Upper Paleozoic tight sandstone reservoir of block A in the eastern margin of Ordos Basin. *China Offshore Oil and Gas*, 34(4), 122-131. DOI: 10.11935/j.issn.1673-1506.2022.04.011.
- Liu, X.Y., Li, S.X., Zhou, X.P., et al. (2023). New fields, new types, and resource potential of petroleum exploration in Ordos Basin. *Acta Petrolei Sinica*, 44(12), 2070-2090. DOI: 10.7623/syxb201312005.
- Luo, X.N., Yi, C., Zhang, Z.L., et al. (2021). Features of clay minerals in the sandstones of middle Jurassic Yan'an Formation of Bayinqingeli-Suhaitu area, northern Ordos Basin. *World Nuclear Geoscience*, 38(02), 162-173. DOI: 10.3969/j.issn.1672-0636.2021.02.004.
- Ma, Y.Q., Lu, Y.C., Liu, S.P., et al. (2015). Characteristics of tight sandstones and forming mechanism of relative high-quality reservoir in Chang 3 member of Yanchang Formation in Xunyi area, Ordos Basin. *Journal of Central South University (Science and Technology)*, 46(08), 3013-3024. DOI: 10.11817/j.issn.1672-7207.2015.08.034.
- Meng, K., Jin, M.B., Wu, B.X. (2019). Jurassic Yan'an Formation reservoir rocks in the Maling oil field, Ordos Basin. *Sedimentary Geology and Tethyan Geology*, 39(03), 73-83.
- Pan, X., Wang, H.H., Wang, Z.L., et al. (2019). Differential Diagenesis of Delta Plain Sandstone and Its Control on Reservoir Classification: A case study on Yan'an Formation in Yinjiacheng area, southwestern Ordos Basin. *Acta Sedimentologica Sinica*, 37(05), 1031-1043. DOI: 10.14027/j.issn.1000-0550.2018.182.
- Pang, J.G., Li, W.H., Guo, J.A., et al. (2021). Diagenesis characteristics and difference analysis of ultra-low permeability and tight sandstone: Taking Yanchang Formation in Longdong area of Ordos Basin as an example. *Chinese Journal of Geology*, 56(01), 121-135. DOI: 10.12017/dzdx.2021.009.
- Shi, J.F., Shi, Y.M., Gao, C.L., et al. (2018). Tight sandstone reservoir clay minerals characteristics and sensitivity analysis: A case study of Chang 6 formation in Zhaizihe area, Wuqi Oilfield, Ordos Basin. *Science Technology and Engineering*, 18(20), 88-95.
- Sun, G.Y., Wang, Z.L., Liu, P.L., et al. (2022). Dissolved micro-pores in alkali feldspar and their contribution to improved properties of tight sandstone reservoirs: A case study from Triassic Chang-63 sub-member, Huaqing area, Ordos Basin. *Oil and Gas Geology*, 43(03), 658-669. DOI: 10.11743/ogg20220314.
- Sun, Y.X., Zhang, T., Ding, W.L., et al. (2022). Application of mercury intrusion method and digital image analysis in quantitative analysis of micro-scale pores in tight sandstone reservoirs: a case study of X block in Wuqi Oil Field, Ordos Basin. *Petroleum Geology and Experiment*, 44(06), 1105-1115. DOI: 10.11781/sydz2022061105.
- Tian, J.F., Gao, Y.L., Zhang, P.B., et al. (2022). Genesis and geological implication of illite coatings of Triassic Yanchang Formation in Ordos Basin. *Lithological Reservoirs*, 34(02), 54-65. DOI: 10.12108/yxyqc.20220205.
- Tong, Q. et al. (2022). Influence of reservoir pore-throat structure heterogeneity on water-flooding seepage: A case study of Yanchang formation in Ordos Basin. *Minerals*, 12, 1243. DOI: 10.3390/min12101243.
- Warren, J.K. (2000) Dolomite: occurrence, evolution and economically important associations. *Earth-Science Reviews*, 52(1-3):1-81.
- Xiao, S.D., Wang, Z.L., Pan, X., et al. (2024). Characteristics and genesis of microscopic pore structure of Yan 8 Member reservoir in Yanwu area. *Fault-Block Oil and Gas Field*, 31(1), 86-105. DOI: 10.6056/dkyqt202401011.

- Yang, Y., Huang, Y.G., Feng, Y.S., et al. (2015). Characteristics of interstitial materials in tight sandstone and its effects on reservoir. *Journal of Southwest Petroleum University (Science & Technology Edition)*, 37(05), 1-8. DOI: 10.11885/j.issn.1674-5086.2013.12.09.31.
- Zeng, C.F., Tian, J.C., Zhang, T., et al. (2015). Characteristics of pre-Jurassic paleogeomorphology and hydrocarbon accumulation regularity in Northern Zhenyuan area. *Fault-Block Oil & Gas Field*, 22(03), 273-277. DOI:10.6056/dkyqt201503001.
- Zhang, H., Liao, M.G., Yao, J.L., et al. (2017). Authigenic minerals and their influences on the petrophysical properties of tight sandstone reservoirs: An example from the Chang-3 oil reservoirs in the Longdong region, Ordos basin. *Sedimentary Geology and Tethyan Geology*, 37(03), 22-31.
- Zhang, H.Y., Li, M., Kang, Y.M., et al. (2021). Reservoir architecture and fine characterization of remaining oil in Chang 3 reservoir in Zhenbei Oilfield, Ordos Basin. *Lithologic Reservoirs*, 33(06), 177-188. DOI: 10.12108/yxyqc.20210618.
- Zhang, J.J., Liu, R.P., Wang, L.J., et al. (2023). The influence and control effect of clay minerals on reservoir sensitivity taking Chang 6 ultra-low permeability sandstone reservoir in Heshui area as an example. *Mineral Exploration*, 14(01), 1-8. DOI: 10.20008/j.kkcc.202301001.
- Zhang, Q., Li, W.H., Liu, W.H., et al. (2021). Jurassic sedimentary systems and paleogeographic evolution of Ordos Basin. *Chinese Journal of Geology*, 56(04), 1106-1119. DOI: 10.12017/dzcx.2021.059.
- Zhang, Q.Z., Sun, Y.N., Wu, D.S., et al. (2019). Influence of unconformity and sandbody configuration on accumulation of hydrocarbon in Chang 3 and above low-permeability reservoirs in Zhenbei area. *Journal of Xi'an Shiyou University (Natural Science Edition)*, 34(05), 31-36. DOI:10.3969/j.issn.1673-064X.2019.05.004.
- Zhang, W.J., Zhao, J., Xi, H., et al. (2020). Identification methods of Chang 3 Member Low Resistivity Pay Zones in Western Zhenbei area of Ordos Basin. *Well Logging Technology*, 44(06), 589-593+600. DOI: 10.16489/j.issn.1004-1338.2020.06.013.
- Zhang, Y., Yang, L.L., Chen, M.Y., et al. (2014). Identification of low-resistivity oil layers in the Yan'an Formation in Zhenbei area by combining array induction invasion factor method with interval transit time- resistivity cross-plot. *Journal of Xi'an Shiyou University (Natural Science Edition)*, 29(03), 8-14+6.
- Zhao, J.R., Zhu, H.H., Feng, X.Z., et al. (2021). Characteristics of Member mica of Yanchang Formation in the Ordos Basin and its effects on reservoirs. *Fault-Block Oil & Gas Field*, 28(02), 194-199. DOI: 10.6056/dkyqt202102009.
- Zhao, X.M., Guo, F., Peng, X.X., et al. (2021). Reservoir characteristics and main controlling factors of Yan 10 sandy braided fluvial facies in Anbian area, Ordos Basin. *Lithologic Reservoirs*, 33(06), 124-134. DOI: 10.12108/yxyqc.20210613.
- Zhong, H.L., Zhang, F.Q., Zhao, Z.Y., et al. (2021). Micro-scale pore – throat distributions in tight sandstone reservoirs and its constrain to movable fluid. *Petroleum Geology and Experiment*, 43(1), 77-85. DOI: 10.11781/sydz202101077.
- Zhou, X.F., Ding, L., Yang, W.G., et al. (2017). Growth pattern of chlorite film in Chang 8 sandstone of Yanchang Formation in Ordos Basin. *Lithologic Reservoirs*, 29(4), 1-10. DOI: 10.3969/j.issn.1673-8926.2017.04.001.
- Zou, C.N., Li, S.X., Xiong, B., et al. (2024). Connotation, pathway, and significance of carbon neutrality "Super Energy System": A case study of the Ordos Basin, NW China. *Petroleum Exploration and Development*, 51(4), 924-936. DOI: 10.11698/PED.20240021.